Nanoscale

Cite this: *Nanoscale*, 2012, **4**, 3444

www.rsc.org/nanoscale

PAPER

Thermo-compressive transfer printing for facile alignment and robust device integration of nanowires†

Won Seok Lee,[a] Sejeong Won,[a] Jeunghee Park,[c] Jihye Lee*[b] and Inkyu Park*[a]

Received 18th February 2012, Accepted 21st March 2012
DOI: 10.1039/c2nr30392b

Controlled alignment and mechanically robust bonding between nanowires (NWs) and electrodes are essential requirements for reliable operation of functional NW-based electronic devices. In this work, we developed a novel process for the alignment and bonding between NWs and metal electrodes by using thermo-compressive transfer printing. In this process, bottom-up synthesized NWs were aligned in parallel by shear loading onto the intermediate substrate and then finally transferred onto the target substrate with low melting temperature metal electrodes. In particular, multi-layer (*e.g.* Cr/Au/In/Au and Cr/Cu/In/Au) metal electrodes are softened at low temperatures (below 100 °C) and facilitate submergence of aligned NWs into the surface of electrodes at a moderate pressure (~5 bar). By using this thermo-compressive transfer printing process, robust electrical and mechanical contact between NWs and metal electrodes can be realized. This method is believed to be very useful for the large-area fabrication of NW-based electrical devices with improved mechanical robustness, electrical contact resistance, and reliability.

1 Introduction

Nanowires (NWs) synthesized by bottom-up fabrication methods such as hydrothermal reaction[1–3] or chemical vapor deposition (CVD)[4,5] have been widely used in transistors,[6] light emitting diodes,[7] sensors,[8–11] solar cells,[12] and power generation devices[13] by integration into device platforms. NW-based devices have been utilizing many advantages of NWs such as their electrical tunability, high light emission efficiency, high surface to volume ratio, and high surface reactivity.

Common methods for the alignment and integration of NWs onto metal electrodes are based on external forces from electric field,[14,18–20] magnetic field,[15] single NW manipulation,[16] *etc.* However, these methods have only enabled physical alignment, not the mechanically robust bonding between NWs and metal electrodes since the bonding is based on weak van der Waals forces. Therefore, post-processes such as focused ion beam (FIB) induced deposition,[17] selective electrodeposition,[18] photolithography,[16,19] and soldering[15,20] were needed to enhance the mechanical and electrical contacts. However, those methods have several drawbacks such as increased process complexity, high process cost, and low manufacturing throughput. In particular, FIB-based deposition[17] is time-consuming and expensive. In the selective electrodeposition process,[18] NWs can possibly react with chemical solutions. In the case of photolithography (or e-beam lithography),[16,19] NWs can be contaminated or damaged by a photoresist (or e-beam resist), developer and solvent. Also, the above-mentioned soldering methods[15,20] were limited to only specialized nanomaterials such as Au/Ni/Au composite NWs and Sn–In based alloy NWs. In order to resolve these issues, direct NW–metal electrode bonding based on the hot-pressing technique[21] was recently introduced as a way of improving the contact characteristics between NWs and electrodes with high yield and a relatively low temperature process condition (180 °C). However, in this case, a high pressure of 96 bar was required and the contact resistance was as high as 1.1×10^{-1} Ω cm^2. In this paper, we present a novel NW integration process based on a thermo-compressive transfer printing of NWs on metal electrodes with lower temperature and pressure requirements by using an alloy of gold (Au) (or copper (Cu)) and indium (In), which is a low melting temperature material. This allows the submergence of NWs into metal electrodes and mechanically robust bonding of NWs onto metal electrodes without the need for additional bonding processes. The method is very fast and simple due to parallel processing of alignment and bonding of NWs onto the metal electrodes. Furthermore, a superb electrical contact property has been achieved as compared to the previously developed hot-pressing method.[21]

[a]*Department of Mechanical Engineering and KI for the NanoCentury, Korea Advanced Institute of Science and Technology (KAIST), Daejeon 305-701, Korea. E-mail: inkyu @kaist.ac.kr; Fax: +82-42-350-3210; Tel: +82-42-350-3233*
[b]*Department of Nano Manufacturing Technology, Korea Institute of Machinery and Materials (KIMM), Daejeon 305-343, Korea. E-mail: jihyelee @kimm.re.kr; Fax: +82-42-868-7123; Tel: +82-42-868-7801*
[c]*Department of Chemistry, Korea University, Jochiwon 339-700, Korea*
† Electronic supplementary information (ESI) available. See DOI: 10.1039/c2nr30392b

2 Experimental

The procedure for thermo-compressive transfer printing is illustrated in Fig. 1. The process was performed in two transfer steps. Firstly, ZnO NWs were grown on a Si(100) donor substrate in random directions as shown in Fig. 1(a) by thermal evaporation using the mixture of ZnO powders (99.9%, Aldrich), graphite powders (<20 microns, Aldrich) and Sn powders (99.8%, Acros). The source (ZnO : graphite : Sn = 1 : 1 : 0.01 by weight%) was loaded in the Al_2O_3 boat and was located at the center of the quartz tube (diameter: 2.5 cm) and the Si substrate was placed 5 cm downstream from the source. After evacuating the quartz tube to $\sim 9 \times 10^{-2}$ Torr by using a rotary pump, the furnace temperature was increased to 900 °C. The ZnO NWs were formed by a reaction between the source and Ar–O_2 mixture gas (Ar: 100 sccm, O_2: 1 sccm), and were highly crystalline with orientation in preferentially the [010] growth direction with a square cross-sectional area (see Fig. S1 in the ESI†). In the first transfer step, the ZnO NWs were transferred to the intermediate Si/SiO_2 substrate as shown in Fig. 1(a) and (b). The donor substrate was flipped over such that the synthesized NWs faced downward, making a contact with the top surface of the intermediate substrate. In this process, we used a contact printing method[22] where a normal pressure of 30 mbar was applied to the intermediate substrate while it was pushed with a constant velocity of 15 mm min^{-1}. In our case, we demonstrated that randomly grown NWs by the CVD method could be aligned by the contact printing method instead of vertically grown NWs as reported by Z. Fan *et al.*[22] The scanning electron microscopy (SEM) image of the aligned ZnO NWs on the intermediate substrate is shown in Fig. 1(a). We could observe that ZnO NWs randomly grown on the donor substrate were aligned in the pushed direction and transferred onto the intermediate substrate with high density and long lengths (10–20 μm). In the second transfer step, the intermediate substrate was cut by 3×5 mm^2 and then the slice of the intermediate substrate was pressed against the target substrate with metal electrodes under thermo-compression conditions (temperature = 23–150 °C; pressure = 5–10 bar) for 5 minutes as shown in Fig. 1(c) and (d). After removing the intermediate substrate from the target substrate, ZnO NWs were aligned and submerged onto the metal electrodes at the same time. This completes the fabrication of ZnO NW-based devices as shown in Fig. 1(e).

We used multi-metal layers (Cr/Au/In/Au and Cr/Cu/In/Au) as the In-rich metal electrodes with low melting temperatures. The thin metal films (Cr/Au/In/Au = 10 nm/30 nm/150 nm/5 nm and Cr/Cu/In/Au = 10 nm/30 nm/150 nm/5 nm from lower to upper layers) were deposited by electron beam evaporation for the source and drain electrodes on a Si(100) substrate with a thermally grown 300 nm thick SiO_2 layer. The top Au layer (5 nm) was deposited on the In electrode layer in order to prevent the indium (In) layer from oxidation by forming an $AuIn_2$ layer on the surface of the metal electrodes.[23] The In layer (150 nm) was used as a soldering material for bonding with ZnO NWs at low temperature and low pressure due to its low melting temperature of 156 °C.

The contact region between NWs and metal electrodes was analyzed by field-emission scanning electron microscopy

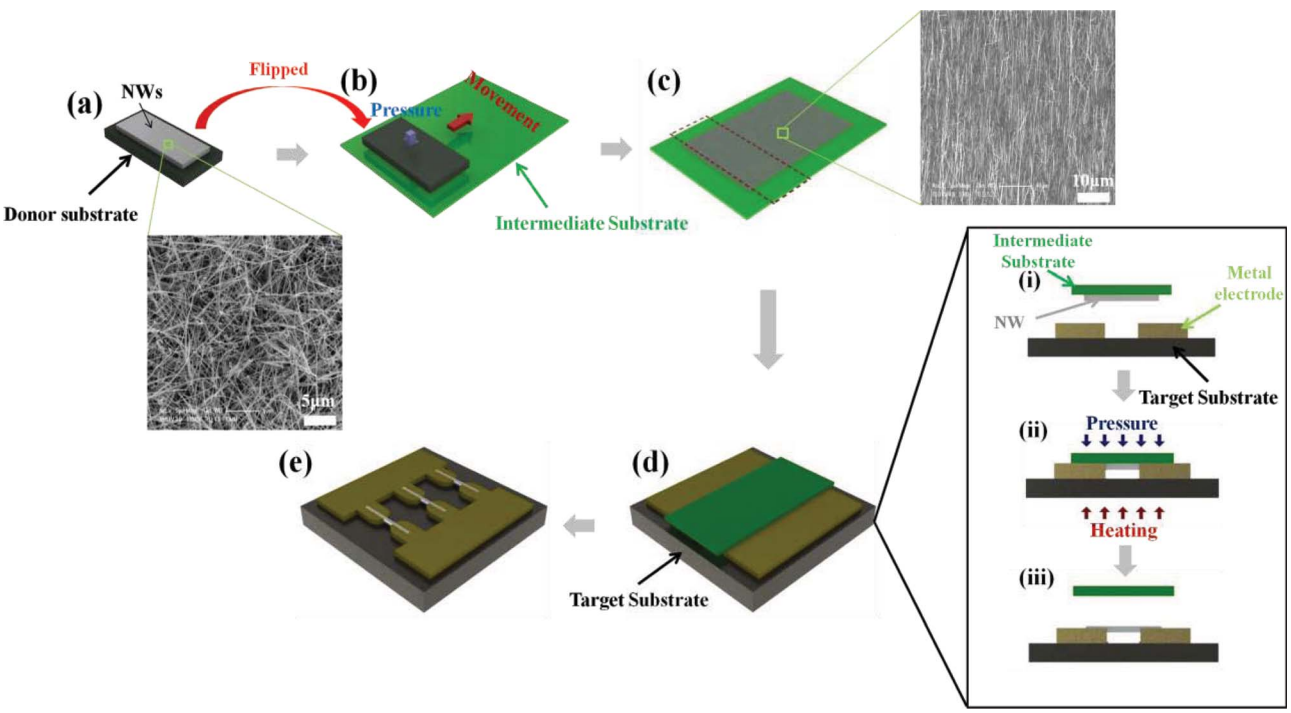

Fig. 1 Process flow of thermo-compressive transfer printing of NWs onto metal electrodes: (a) randomly grown ZnO NWs on Si substrate (donor substrate); SEM image of synthesized NWs is shown. (b) First transfer printing of NWs onto Si/SiO_2 substrate (intermediate substrate), (c) ZnO NWs transferred to the intermediate substrate; SEM image of transferred and aligned NWs is shown. The intermediate substrate was cut appropriately for the second transfer as shown by the dotted line. (d) Second transfer printing of ZnO NWs from the intermediate substrate to the target substrate (Si/SiO_2) with a pair of metal electrodes under thermal compression. (e) Finally fabricated ZnO NW-based device.

(FE-SEM, Sirion), Cs-Corrected Scanning Transmission Electron microscopy (Cs-Corrected STEM, JEM-ARM200F), and X-ray diffraction (XRD, Rigaku D/MAX-2500). Electrical characteristics and bonding strength were measured by using a semiconductor analyzer (Keithley 4200-SCS) and lateral force microscope (LFM, XE-100), respectively.

3 Results and discussion

Fig. 2(a) shows the results of thermo-compressive transfer printing on Cr/Au/In/Au metal electrodes at different pressure and temperature conditions. At the room temperature (23 °C), ZnO NWs were not observed to remain between metal electrodes. Even with higher pressure (10 bar), ZnO NWs did not remain while metal electrodes were deformed in the lateral direction and had some pressure marks of NWs on the surface. At 100 °C, we could observe that ZnO NWs were embedded into metal electrodes under pressures of both 5 bar and 10 bar. It is presumed that ZnO NWs were easily embedded and bonded to metal electrodes due to the softening and plastic deformation of metal electrodes. However, when the temperature reached 150 °C, metal electrodes were severely deformed and some parts of them were detached from the target substrate to the intermediate substrate. The possible reason for this result is that the ductility of the In-rich metal electrode was much greater at 150 °C (near the melting temperature of In). As a consequence, the contact area between the intermediate substrate and metal electrode was increased and this caused a strong attractive force between them.[24] Therefore, when the intermediate substrate was detached from the metal electrode after the thermo-compression process at 150 °C, the cohesive fracture in the metal electrode or adhesive fracture between Si/SiO_2 and the metal electrode could have happened due to the increased adhesive energy between the intermediate substrate and metal electrode. We assumed that this is the reason why the metal electrode was partially detached from the target substrate to the intermediate substrate at 150 °C. However, the detailed mechanism will be further studied in the future by an in-depth analysis of adhesive and cohesive failure of interfaces between the intermediate substrate, metal electrode, and target substrate under various temperature conditions.

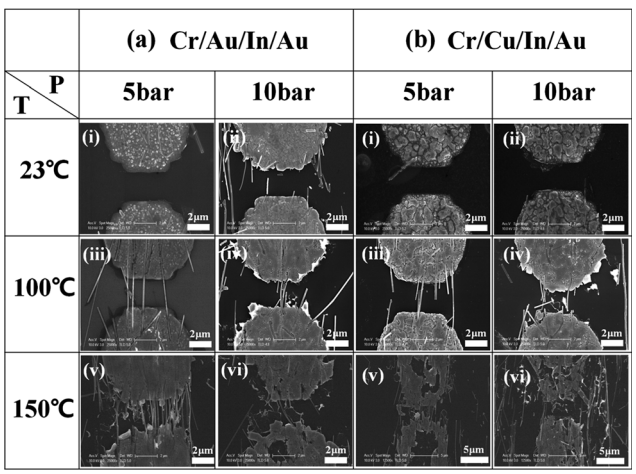

Fig. 2 Results of thermo-compressive transfer printing under various temperature and pressure conditions on metal electrodes of (a) Cr/Au/In/Au and (b) Cr/Cu/In/Au. (i) and (ii) bonding of ZnO NWs on metal electrodes could not be achieved at a low temperature (23 °C). (v) and (vi) Metal electrodes were deformed severely and detached from the target substrate to the intermediate substrate at a high temperature (150 °C). (iii) and (iv) ZnO NWs could be embedded into metal electrodes at an optimal temperature (100 °C). However, metal electrodes were more severely deformed at 10 bar (iv) than at 5 bar (iii).

The results of thermo-compressive transfer printing with the Cr/Cu/In/Au metal electrodes are shown in Fig. 2(b). Process parameters, pressure and temperature, had the same effect on the transfer and bonding results with the Cr/Au/In/Au metal electrodes. At the temperature of 100 °C under a pressure of 5 bar, ZnO NWs were observed to be embedded into electrodes without causing severe deformation of electrodes in the lateral direction. We found that the pressure of 5 bar and temperature of 100 °C are optimal conditions for both Cr/Au/In/Au and Cr/Cu/In/Au electrodes. Severe damage of electrodes is observed at 150 °C for Cr/Cu/In/Au metal electrodes, similar to Cr/Au/In/Au electrodes as shown in Fig. 2(b-v and vi).

The contact region of ZnO NW with the Cr/Au/In/Au metal electrode was investigated by using TEM and high resolution TEM (HRTEM) analysis as shown in Fig. 3(a) and (b). It is shown that ZnO NW was completely embedded into the metal electrode and formed a conformal contact with the metal electrode without any voids. This can be attributed to the softening of the metal electrode at 100 °C. Energy dispersive spectrometer (EDS) analysis of the cross-section on the contact region of the metal electrode and ZnO NW shows that both Au and In are present in the whole metal electrode area as shown in Fig. 3(a). The XRD result shown in Fig. 3(c) shows that Au and In exist in the form of both $AuIn_2$ and In. All Au in the metal electrode has been transformed into $AuIn_2$, which can be attributed to the spontaneous alloy formation between Au and In at room temperature.[25,26] However, some In remains without reacting with Au because of an excessive amount of In in the multi-metallic electrode layers. Therefore, in the thermo-compressive bonding process, ZnO NWs form contacts with both $AuIn_2$ and In. Similar results for thermo-compressive bonding onto Cr/Cu/In/Au metal electrodes are provided in Fig. S2 in the ESI†.

The bonding strength between ZnO NW and metal electrodes was measured by applying a lateral displacement at the center of the ZnO NW using LFM[27] and the results are shown in Fig. 4. Different failure phenomena for the samples fabricated by thermo-compressive transfer printing and contact printing can be observed by looking at the atomic force microscope (AFM) images taken before and after LFM tests. In the case of ZnO NWs bonded onto Cr/Au/In/Au metal electrodes by thermo-compressive transfer printing at 100 °C and 5 bar, the failure occurred at a force of 0.9 μN by the breakage of ZnO NW, instead of the metal electrode–NW contact region. The shear stress at the metal electrode–NW interface was calculated from a numerical simulation (see Fig. S3 in the ESI†). When the breakage of the ZnO NW occurred, the maximum local shear stress was 2.92 GPa at the edge of the bonding surface between the metal electrode and NW. However, the average shear stress of the bonding surface was 22.7 MPa since most of the bonding surface was under very low stress (*e.g.* 0.45 MPa and 15 kPa at 1 μm and 1.5 μm from the edge, respectively). This indicates that

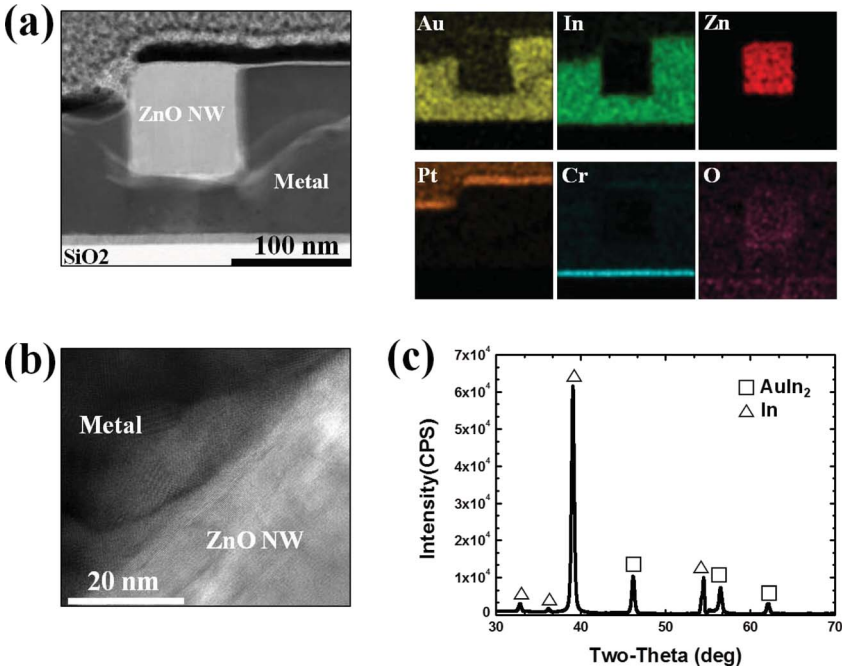

Fig. 3 Microstructural characterization of ZnO NWs on Cr/Au/In/Au electrode bonded by thermo-compressive transfer printing. (a) TEM image and EDS analysis of the cross-section of the contact between ZnO NW and the metal electrode. TEM image shows ZnO NW was well embedded into the metal electrode and EDS analysis shows the component of the metal electrode with a uniform distribution of Au and In throughout the entire depth of the electrode. (b) HRTEM image of the contact region. Bonding of ZnO NW and the metal electrode without voids can be clearly observed. (c) XRD analysis of the Cr/Au/In/Au metal electrode. The peaks of both In and $AuIn_2$ can be detected, which indicates the formation of an alloy of In and Au in the metal electrode.

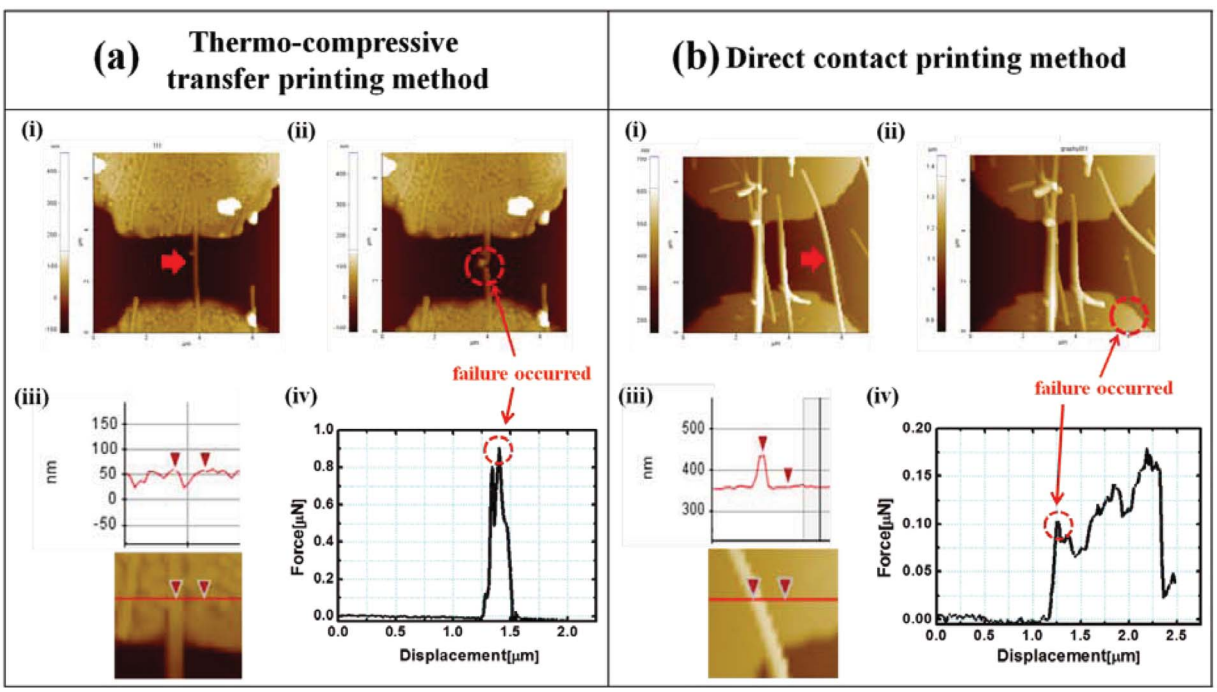

Fig. 4 Characterization of the mechanical strength of NW–electrode bonding by lateral force microscopy (LFM). Atomic force microscope (AFM) images of (a) ZnO NW bonded by thermo-compressive transfer printing on the Cr/Au/In/Au electrode and (b) ZnO NW bonded by contact printing on the Cr/Au electrode. (i) Before and (ii) after applying lateral displacement to the ZnO NWs in the pointed direction; (iii) line profile of metal electrode bonded ZnO NWs; (iv) plot of force *versus* displacement in the LFM measurement.

the bonding strength of the metal electrode and NW by thermo-compressive transfer printing exceeds an average of 22.7 MPa at least and is strong enough to withstand the maximum local shear stress (2.92 GPa) at the edge. As shown both in the TEM (Fig. 3(a)) and AFM (Fig. 4(a-iii)) images, the ZnO NW was embedded into the Cr/Au/In/Au metal electrode during the second transfer printing by heat and pressure and this has resulted in a high bonding strength. In contrast, when the ZnO NW was bonded onto the Au metal electrode by conventional contact printing, failure happened at the metal electrode–NW interface by a force of 0.1 μN. The maximum local shear stress generated at the edge of the bonding surface between the metal electrode and ZnO NW estimated from the numerical simulation was 562 MPa and the average shear stress of the bonding surface was 4.1 MPa when the failure of the metal electrode–NW contact occurred (see Fig. S3(b) in the ESI†). This failure was caused by a low bonding strength which could not withstand the maximum local shear stress (562 MPa) and average shear stress (4.1 MPa). Therefore, the crack at the metal electrode–NW interface could be initiated at the edge and propagated to result in a complete fracture of the bonding surface. As shown in Fig. 4(b-iii), the NW was positioned on the top surface of the Au electrode, not forming an embedded structure. Therefore, a weak van der Waals force at the contacting surface provides limited bonding strength as mentioned above. From these results, we can conclude that the thermo-compressive transfer printing provides superior bonding strength (>22.7 MPa) between NWs and metal electrodes as compared to the conventional contact printing process (4.1 MPa). In other words, mechanically robust bonding between NWs and metal electrodes is enabled by our thermo-compressive transfer printing process.

We could also find from the electrical measurement that the bonding between Cr/Au/In/Au metal electrodes and ZnO NWs gives rise to ohmic contact properties as shown in Fig. 5. It is presumed that ZnO NW formed contacts with both In and $AuIn_2$ when it was embedded into the metal electrode, by observing the TEM-EDS mapping and XRD peaks of the metal electrode (Fig. 3). In order to form a good ohmic contact between a metal and n-type semiconductor materials, the work function of metal electrodes should be close to or lower than the electron affinity of the semiconductor.[28] The contact of In and ZnO NW formed an ohmic contact because the work function of In is 4.09 eV and the electron affinity of ZnO NW is 4.2–4.35 eV. The specific contact resistance (ρ_c) could be calculated from two different resistances at different gap sizes of 2 μm and 4 μm as shown in Fig. 5(b), resulting in a specific contact resistance of $\rho_c = 3.04 \times 10^{-5}$ Ω cm^2. This value suggests that the contact between the ZnO NW and the metal electrode was well bonded with much lower specific contact resistance than that for the Al–ZnO NW bonding by the hot-pressing process[21] ($\rho_c = 1.1 \times 10^{-1}$ Ω cm^2). Also, this value is comparable to $\rho_c = 1.1 \times 10^{-5}$ Ω cm^2 for Pt–ZnO NW bonding by using a focused ion beam (FIB) deposition of Pt.[29] Fig. 5(c) and (d) show the characterization of a ZnO NW-based field effect transistor (FET) fabricated by using our thermo-compressive transfer printing process. The figure shows an n-type semiconductor property at different gate voltages. As shown in Fig. 5(c), the threshold voltage is as high as approximately −40 V, which can be attributed to the existence of air gap (~100 nm) between the ZnO NW and SiO_2 surface. Y.-K. Chang and F.C.-N. Hong reported[21] that an air gap between NWs and dielectric surface can cause a high threshold voltage. Other reasons for the high negative threshold voltage could be the large thickness of the SiO_2 layer (~300 nm) and high n-type doping of our ZnO NWs by Sn (1–2%) (see Fig. S4 and S5, and Table S1 in the ESI†), which increases the amount of mobile charge carriers (*i.e.* electrons). It is expected that the threshold voltage of the FET device can be reduced by using lightly doped semiconductor NWs, thinner dielectric layer, and thinner metal electrode. Similar device characteristics for the ZnO NW FET device using the Cr/Cu/In/Au electrode by thermo-compressive bonding are given in Fig. S6 in the ESI†.

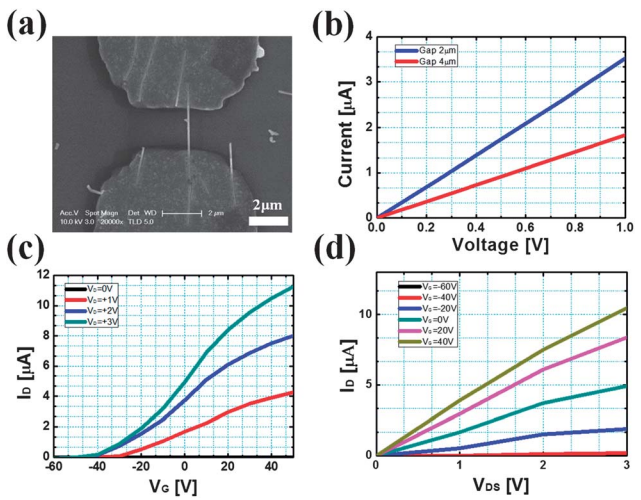

Fig. 5 Electrical characterization of a single ZnO NW FET device fabricated by the thermo-compressive transfer printing process. (a) SEM image of a single ZnO NW device using the Cr/Au/In/Au electrode. (b) I_D–V_{DS} curve for two different gap sizes (2 μm and 4 μm). Specific contact resistance of 3.04×10^{-5} Ω cm^2 can be obtained from these measurements. (c) I_D–V_G curves at different V_{DS}s and (d) I_D–V_{DS} curve at different V_Gs. It shows the behavior of an n-type semiconductor and threshold voltage of approximately −40 V.

4 Conclusions

In summary, we have demonstrated a novel method for the simultaneous alignment and robust bonding of NWs onto metal electrodes by using a very simple two-step thermo-compressive transfer printing technique. ZnO NWs could be embedded into metal electrodes of Cr/Au/In/Au and Cr/Cu/In/Au with low melting temperatures by the thermo-compressive transfer printing process. This resulted in mechanically robust bonding and stable ohmic contact between NWs and metal electrodes. Our method for ZnO NW–metal electrode bonding provided much lower contact resistance than the hot-pressing method and is comparable to the FIB-deposition method. Furthermore, mechanically robust bonding was demonstrated by using LFM. Although we demonstrated the applicability of this process to only ZnO NWs in this work, we believe it can be used for diverse 1D nanomaterials by designing appropriate process conditions and material properties (*e.g.* modulation of work functions by doping control). We believe that this method will be very useful for the large-area fabrication of mechanically robust NW-based electrical devices such as field effect transistors, light emitting

diodes, and sensors due to the advantages of fast, low-cost, and parallel manufacturing without the need for additional post-processing steps.

Acknowledgements

This research was supported by the Future-based Technology Development Program (Nano Fields) (2009-0082527) and Basic Science Research Program (2011-0004409) through the National Research Foundation of Korea (NRF) funded by the Korean government (MEST). The authors would like to thank Mr Chan-Woong Na for providing ZnO nanowires and Mr Yun-Chang Park at the National Nanofab Center (NNFC) for valuable discussion.

References

1 Z.-Y. Yuan, X.-B. Zhang and B.-L. Su, *Appl. Phys. A: Mater. Sci. Process.*, 2004, **78**, 1063–1066.
2 L. E. Greene, M. Law, J. Goldberger, F. Kim, J. C. Johnson, Y. Zhang, R. J. Saykally and P. Yang, *Angew. Chem., Int. Ed.*, 2003, **42**, 3031–3034.
3 Y. Li, J. Wang, Z. Deng, Y. Wu, X. Sun, D. Yu and P. Yang, *J. Am. Chem. Soc.*, 2001, **123**, 9904–9905.
4 C.-C. Chen and C.-C. Yeh, *Adv. Mater.*, 2000, **12**, 738–741.
5 S.-W. Kim, S. Fujita and S. Fujita, *Appl. Phys. Lett.*, 2005, **86**, 153119.
6 Y. Cui, Z. Zhong, D. Wang, W. U. Wang and C. M. Lieber, *Nano Lett.*, 2003, **3**, 149–152.
7 J. Bao, M. A. Zimmler and F. Capasso, *Nano Lett.*, 2006, **6**, 1719–1722.
8 Q. Wan, Q. H. Li, Y. J. Chen, T. H. Wang, X. L. He, J. P. Li and C. L. Lin, *Appl. Phys. Lett.*, 2004, **84**, 3654.
9 Y. Chen, X. Wang, S. Erramilli, P. Mohanty and A. Kalinowski, *Appl. Phys. Lett.*, 2006, **89**, 223512.
10 P.-H. Yeh, Z. Li and Z. L. Wang, *Adv. Mater.*, 2009, **21**, 4975–4978.
11 S. Bai, W. Wu, Y. Qin, N. Cui, D. J. Bayerl and X. Wang, *Adv. Funct. Mater.*, 2011, **21**, 4464–4469.
12 L. Tsakalakos, J. Balch, J. Fronheiser, B. A. Korevaar, O. Sulima and J. Rand, *Appl. Phys. Lett.*, 2007, **91**, 233117.
13 R. Yang, Y. Qin, L. Dai and Z. L. Wang, *Nat. Nanotechnol.*, 2009, **4**, 34–39.
14 J. Suehiro, N. Nakagawa, S.-I. Hidaka, M. Ueda, K. Imasaka, M. Higashihata, T. Okada and M. Hara, *Nanotechnology*, 2006, **17**, 2567–2573.
15 H. Ye, Z. Gu, T. Yu and D. H. Gracias, *IEEE Trans. Nanotechnol.*, 2006, **5**, 62–66.
16 Q. Li, S.-M. Koo, C. A. Richter, M. D. Edelstein, J. E. Bonevich, J. J. Kopanski, J. S. Suehle and E. M. Vogel, *IEEE Trans. Nanotechnol.*, 2007, **6**, 256–262.
17 C. S. Lao, J. Liu, P. Gao, L. Zhang, D. Davidovic, R. Tummala and Z. L. Wang, *Nano Lett.*, 2006, **6**, 263–266.
18 S. Ingole, P. Aella, S. J. Hearne and S. T. Picraux, *Appl. Phys. Lett.*, 2007, **91**, 033106.
19 D.-I. Suh, S.-Y. Lee, J.-H. Hyung, T.-H. Kim and S.-K. Lee, *J. Phys. Chem. C*, 2008, **112**, 1276–1281.
20 X. Li, E. Chin, H. Sun, P. Kurup and Z. Gu, *Sens. Actuators, B*, 2010, **148**, 404–412.
21 Y.-K. Chang and F. C.-N. Hong, *Nanotechnology*, 2009, **20**, 235202.
22 Z. Fan, J. C. Ho, Z. A. Jacobson, R. Yerushalmi, R. L. Alley, H. Razavi and A. Javey, *Nano Lett.*, 2008, **8**, 20–25.
23 V. Simic and Z. Marinkovic, *Thin Solid Films*, 1992, **209**, 181–187.
24 D. Maugis, *Wear*, 1980, **62**, 349–386.
25 V. Simic and Z. Marinkovic, *Thin Solid Films*, 1977, **41**, 57–61.
26 J. Bjontegaard, L. Buene, T. Finstad, O. Lonsjo and T. Olsen, *Thin Solid Films*, 1983, **101**, 253–262.
27 B. Wu, A. Heidelberg and J. J. Boland, *Nat. Mater.*, 2005, **4**, 525–529.
28 L. J. Brillson and Y. Lu, *J. Appl. Phys.*, 2011, **109**, 121301.
29 J. H. He, P. H. Chang, C. Y. Chen and K. T. Tsai, *ECS Trans.*, 2009, **16**, 13–20.